

# Deconvolution in Astronomy: A Review

J.L. Starck

*Service d'Astrophysique, SAP/SEDI, CEA-Saclay, F-91191 Gif-sur-Yvette Cedex, France.*

`jstarck@cea.fr`

E. Pantin

*Service d'Astrophysique, SAP, CEA-Saclay, F-91191 Gif-sur-Yvette Cedex, France.*

`epantin@cea.fr`

and

F. Murtagh

*School of Computer Science, Queen's University Belfast, Belfast BT7 1NN, Northern  
Ireland, and*

*Observatoire de Strasbourg, Université Louis Pasteur, F-67000 Strasbourg, France*

`f.murtagh@qub.ac.uk`

## ABSTRACT

This article reviews different deconvolution methods. The all-pervasive presence of noise is what makes deconvolution particularly difficult. The diversity of resulting algorithms reflects different ways of estimating the true signal under various idealizations of its properties. Different ways of approaching signal recovery are based on different instrumental noise models, whether the astronomical objects are point-like or extended, and indeed on the computational resources available to the analyst. We present a number of recent results in this survey of signal restoration, including in the areas of super-resolution and dithering. In particular we show that most recent published work has consisted of incorporating some form of multiresolution in the deconvolution process.

*Subject headings:* techniques: image processing, methods: data analysis

## 1. Introduction

Deconvolution is a key area in signal and image processing. It is used for objectives in signal and image processing which include the following:

1. Deblurring.
2. Removal of atmospheric seeing degradation.
3. Correction of mirror spherical aberration.
4. Image sharpening.
5. Mapping detector response characteristics to those of another.
6. For image or signal zooming.
7. Optimizing display.

In this article we are focusing on one particular but central interface between model and observational data. In observational astronomy, modeling embraces instrument models, and also information registration and correlation between different data modalities, including image and catalog. The measure of observing performance which is of greatest interest to us in this context is the instrument degradation function, or point spread function. How the point spread function is used to improve image or signal quality lies in deconvolution. We will review a range of important recent results in deconvolution. A central theme for us is how nearly all deconvolution methods, arising from different instrument noise models or from priority given to point source or extended objects, now incorporate resolution scale into their algorithms. Some other results are very exciting too. A recent result of importance is the potential for super-resolution, characterized by a precise algorithmic definition of the “near-black object”. A further result of note is dithering as a form of stochastic resonance, and not just as a purely ad hoc approach to getting a better signal.

Deconvolution of astronomical images has proven in some cases to be crucial for extracting scientific content. For instance, IRAS images can be efficiently reconstructed thanks to a new pyramidal maximum entropy algorithm (Bontekoe et al. 1994). Io volcanism can be studied with a lower resolution of 0.15 arcsec, or 570 km on Io (Marchis et al. 2000). Deconvolved mid-infrared images at 20  $\mu\text{m}$  revealed the inner structure of the AGN in NGC1068, hidden at lower wavelength because of the high extinction (Alloin et al. 2000) (see Fig. 1). Research on gravitational lenses is easier and more efficient when applying deconvolution methods (Courbin et al. 1998). A final example is the high resolution (after deconvolution)

of mid-infrared images revealing the intimate structure of young stellar objects (Zavagno et al. 1999). Deconvolution will be even more crucial in the future in order to fully take advantage of increasing numbers of high-quality ground-based telescopes, for which images are strongly limited in resolution by the seeing.

HST provided a leading example of the need for deconvolution, in the period before the detector system was refurbished. Two proceedings (White and Allen 1991; Hanisch and White 1994) provide useful overviews of this work, and a later reference is (Adorf et al. 1995). While an atmospheric seeing point spread function (PSF) may be relatively tightly distributed around the mode, this was not the case for the spherically aberrated HST PSF. Whenever the PSF “wings” are extended and irregular, deconvolution offers a straightforward way to mitigate the effects of this and to upgrade the core region of a point source. One usage of deconvolution of continuing importance is in information fusion from different detectors. For example, (Faure et al. 2002) deconvolve HST spectra when correlating with ground-based observations. In (Radomski et al. 2002), Keck data are deconvolved, for study with HST data. VLT spectra are deconvolved in (Burud et al. 2002), with other ESO and HST data used as well. In planetary work, (Coustenis et al. 2001) discuss CFHT data as well as HST and other observations.

What emerges very clearly from this small sample – which is in no way atypical – is that a major use of deconvolution is to help in cross-correlating image and signal information.

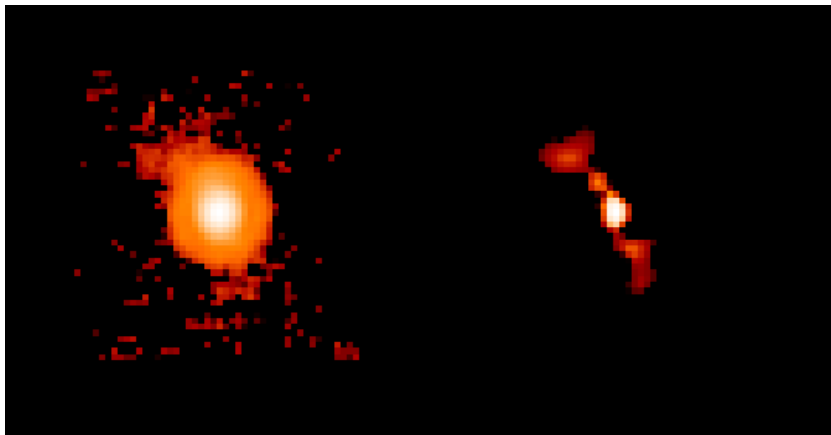


Fig. 1.— The active galaxy nucleus of NGC1068 observed at  $20\ \mu\text{m}$ . Left: the raw image is highly blurred by telescope diffraction. Right: the restored image using the multiscale entropy method reveals the inner structure in the vicinity of the nucleus.

An observed signal is never in pristine condition, and improving it involves inverting the spoiling conditions, i.e. finding a solution to an inverse equation. Constraints related to

the type of signal we are dealing with play an important role in the development of effective and efficient algorithms. The use of constraints to provide for a stable and unique solution is termed regularization. Examples of commonly-used constraints include a result image or signal which is non-negative everywhere, an excellent match to source profiles, necessary statistical properties (Gaussian distribution, no correlation, etc.) for residuals, and absence of specific artifacts (ringing around sources, blockiness, etc.).

Our review opens in section 2 with a formalization of the problem. Section 3 considers the issue of regularization. In section 4, the CLEAN method which is central to radio astronomy is described. Bayesian modeling and inference in deconvolution is reviewed in section 5. Section 6 introduces wavelet-based methods as used in deconvolution. These methods are based on multiple resolution or scale. In sections 7 and 8, important issues related to resolution of the output result image are discussed. Section 7 is based on the fact that it is normally not worthwhile to target an output result with better resolution than some limit, for instance a pixel size. Section 8 investigates when, where and how missing information can be inferred to provide super-resolution.

## 2. The Deconvolution Problem

Noise is the bane of the image analyst’s life. Without it we could so much more easily rectify data, compress it, and interpret it. Unfortunately however deconvolution becomes a difficult problem due to the presence of noise in high-quality or deep imaging.

Consider an image characterized by its intensity distribution (the “data”)  $I$ , corresponding to the observation of a “real image”  $O$  through an optical system. If the imaging system is linear and shift-invariant, the relation between the data and the image in the same coordinate frame is a convolution:

$$\begin{aligned} I(x, y) &= \int_{x_1=-\infty}^{+\infty} \int_{y_1=-\infty}^{+\infty} P(x - x_1, y - y_1) O(x_1, y_1) dx_1 dy_1 \\ &\quad + N(x, y) \\ &= (P * O)(x, y) + N(x, y) \end{aligned} \tag{1}$$

$P$  is the point spread function, PSF, of the imaging system, and  $N$  is additive noise.

In Fourier space we have:

$$\hat{I}(u, v) = \hat{O}(u, v) \hat{P}(u, v) + \hat{N}(u, v) \tag{2}$$

We want to determine  $O(x, y)$  knowing  $I$  and  $P$ . This inverse problem has led to a large amount of work, the main difficulties being the existence of: (i) a cut-off frequency

of the point spread function, and (ii) the additive noise. See for example (Cornwell 1989; Katsaggelos 1993; Bertero and Boccacci 1998; Molina et al. 2001).

A solution can be obtained by computing the Fourier transform of the deconvolved object  $\hat{O}$  by a simple division between the image  $\hat{I}$  and the PSF  $\hat{P}$

$$\hat{\tilde{O}}(u, v) = \frac{\hat{I}(u, v)}{\hat{P}(u, v)} = \hat{O}(u, v) + \frac{\hat{N}(u, v)}{\hat{P}(u, v)} \quad (3)$$

This method, sometimes called the *Fourier-quotient method*, is very fast. We only need to do a Fourier transform and an inverse Fourier transform. For frequencies close to the frequency cut-off, the noise term becomes important, and the noise is amplified. Therefore in the presence of noise, this method cannot be used.

Eqn. 1 is usually in practice an ill-posed problem. This means that there is no unique and stable solution.

The diversity of algorithms, to be looked at in the following sections, reflects different ways of recovering a “best” estimate of the source. If one has good prior knowledge, then simple modeling of PSF-convolved sources with a set of variable parameters is often used. In fact, this is often a favored approach, in order to avoid deconvolution, even though its users are unaware of the consequences of its spatially-correlated residuals. Lacking specific source information, one then relies on general properties which have been referred to in section 1. The algorithms described in our review will approach these issues in different ways.

With linear regularized methods (section 3) we use a smoothing/sharpening trade-off. CLEAN assumes our objects are point sources. We discuss the powerful Bayesian methodology in terms of different noise models which can be applicable. Maximum entropy makes a very specific assumption about source structure, but in at least its traditional formulations was poor at addressing the expected properties of the residuals produced when the estimated source was compared to the observations. Some further work is reviewed which models planetary images, or extended objects. So far, all of these methods work, usually iteratively, on the given data.

The story of the following section, section 6, is then an answer to the question: Where and how do we introduce resolution scale into the methods which we have reviewed in sections 3, 4 and 5, and what are the benefits of doing this?

Some varied directions that deconvolution can take are as follows:

- Super-resolution: object spatial frequency information outside the spatial bandwidth of the image formation system is recovered.

- Blind deconvolution: the PSF  $P$  is unknown.
- Myopic deconvolution: the PSF  $P$  is partially known.
- Image reconstruction: an image is formed from a series of projections (computed tomography, positron emission tomography or PET, and so on).

We will discuss only the deconvolution and super-resolution problems in this paper.

In the deconvolution problem, the PSF is assumed to be known. In practice, we have to construct a PSF from the data, or from an optical model of the imaging telescope. In astronomy, the data may contain stars, or one can point towards a reference star in order to reconstruct a PSF. The drawback is the “degradation” of this PSF because of unavoidable noise or spurious instrument signatures in the data. So, when reconstructing a PSF from experimental data, one has to reduce very carefully the images used (background removal for instance) or otherwise any spurious feature in the PSF would be repeated around each object in the deconvolved image. Another problem arises when the PSF is highly variable with time, as is the case for adaptive optics images. This means usually that the PSF estimated when observing a reference star, after or before the observation of the scientific target, has small differences from a perfect PSF. In this particular case, one has to turn towards myopic deconvolution methods (Christou et al. 1999) in which the PSF is also estimated in the iterative algorithm using a first guess deduced from observations of reference stars.

Another approach consists of constructing a synthetic PSF. Several studies (Buonanno et al. 1983; Moffat 1969; Djorgovski 1983; Molina et al. 1992) have suggested a radially symmetric approximation to the PSF:

$$P(r) \propto \left(1 + \frac{r^2}{R^2}\right)^{-\beta} \quad (4)$$

The parameters  $\beta$  and  $R$  are obtained by fitting the model with stars contained in the data.

### 3. Linear Regularized Methods

It is easy to verify that the minimization of  $\| I(x, y) - P(x, y) * O(x, y) \|^2$  leads to the least square solution:

$$\hat{\tilde{O}}(u, v) = \frac{\hat{P}^*(u, v)\hat{I}(u, v)}{|\hat{P}(u, v)|^2} \quad (5)$$

which is defined only if  $\hat{P}(u, v)$  (the Fourier transform of the PSF) is different from zero. A tilde indicates an estimate. The problem is generally ill-posed and we need to introduce *regularization* in order to find a unique and stable solution.

Tikhonov regularization (Tikhonov et al. 1987) consists of minimizing the term:

$$J_T(O) = \| I(x, y) - (P * O)(x, y) \|^2 + \lambda \| H * O \|^2 \quad (6)$$

where  $H$  corresponds to a high-pass filter. This criterion contains two terms. The first,  $\| I(x, y) - P(x, y) * O(x, y) \|^2$ , expresses fidelity to the data  $I(x, y)$ , and the second,  $\lambda \| H * O \|^2$ , expresses smoothness of the restored image.  $\lambda$  is the regularization parameter and represents the trade-off between fidelity to the data and the smoothness of the restored image. The solution is obtained directly in Fourier space:

$$\hat{O}(u, v) = \frac{\hat{P}^*(u, v) \hat{I}(u, v)}{|\hat{P}(u, v)|^2 + \lambda |\hat{H}(u, v)|^2} \quad (7)$$

Finding the optimal value  $\lambda$  necessitates use of numerical techniques such as cross-validation (Golub et al. 1979; Galatsanos and Katsaggelos 1992). This method works well, but computationally it is relatively lengthy and produces smoothed images. This second point can be a real problem when we seek compact structures such as is the case in astronomical imaging.

This regularization method can be generalized, and we write:

$$\hat{O}(u, v) = \hat{W}(u, v) \frac{\hat{I}(u, v)}{\hat{P}(u, v)} \quad (8)$$

which leads directly to Wiener filtering when the  $W$  filter depends on both signal and noise behavior (see equation (16) below which introduces Wiener filtering in a Bayesian framework).  $W$  must satisfy the following conditions (Bertero and Boccacci 1998). We give here the window definition in 1D.

1.  $|\hat{W}(\nu)| \leq 1$ , for any  $\nu > 0$
2.  $\lim_{\nu \rightarrow 0} \hat{W}(\nu) = 1$  for any  $\nu$  such that  $\hat{P}(\nu) \neq 0$
3.  $\hat{W}(\nu)/\hat{P}(\nu)$  bounded for any  $\nu > 0$

Any function satisfying these three conditions defines a regularized linear solution. The most commonly used windows are Gaussian, Hamming, Hanning, and Blackman (Bertero

and Boccacci 1998). The function can also be derived directly from the PSF (Pijpers 1999). Linear regularized methods have the advantage of being very attractive from a computation point of view. Furthermore, the noise in the solution can easily be derived from the noise in the data and the window function. For example, if the noise in the data is Gaussian with a standard deviation  $\sigma_d$ , the noise in the solution is  $\sigma_s^2 = \sigma_d^2 \sum W_k^2$ . But this noise estimation does not take into account errors relative to inaccurate knowledge of the PSF, which limits its interest in practice.

Linear regularized methods present also a number of severe drawbacks:

- Creation of Gibbs oscillations in the neighborhood of the discontinuities contained in the data. The visual quality is therefore degraded.
- No a priori information can be used. For example, negative values can exist in the solution, while in most cases we know that the solution must be positive.
- Since the window function is a low-pass filter, the resolution is degraded. There is trade-off between the resolution we want to achieve and the noise level in the solution. Other methods such as wavelet-based methods do not have such a constraint.

#### 4. CLEAN

The CLEAN method (Högbom 1974) is a mainstream one in radio astronomy. This approach assumes the object is only composed of point sources. It tries to decompose the image (called the dirty map) into a set of  $\delta$ -functions. This is done iteratively by finding the point with the largest absolute brightness and subtracting the PSF (dirty beam) scaled with the product of the loop gain and the intensity at that point. The resulting residual map is then used to repeat the process. The process is stopped when some prespecified limit is reached. The convolution of the  $\delta$ -functions with an ideal PSF (clean beam) plus the residual equals the restored image (clean map). This solution is only possible if the image does not contain large-scale structures.

In the work of Champagnat et al. (1996) and Kaaresen (1997), the restoration of an object composed of peaks, called *sparse spike trains*, has been treated in a rigorous way.



## 5. Bayesian Methodology

### 5.1. Definition

The Bayesian approach consists of constructing the conditional probability density relationship:

$$p(O | I) = \frac{p(I | O)p(O)}{p(I)} \quad (9)$$

where  $p(I)$  is the probability of our image data and  $p(O)$  is the probability of the real image, over all possible image realizations. The Bayes solution is found by maximizing the right part of the equation. The maximum likelihood solution (ML) maximizes only the density  $p(I | O)$  over  $O$ :

$$\text{ML}(O) = \max_O p(I | O) \quad (10)$$

The maximum-a-posteriori solution (MAP) maximizes over  $O$  the product  $p(I | O)p(O)$  of the ML and a prior:

$$\text{MAP}(O) = \max_O p(I | O)p(O) \quad (11)$$

$p(I)$  is considered as a constant value which has no effect in the maximization process, and is ignored. The ML solution is equivalent to the MAP solution assuming a uniform probability density for  $p(O)$ .

### 5.2. Maximum Likelihood with Gaussian Noise

The probability  $p(I | O)$  is

$$p(I | O) = \frac{1}{\sqrt{2\pi}\sigma_N} \exp -\frac{(I - P * O)^2}{2\sigma_N^2} \quad (12)$$

and, assuming that  $p(O)$  is a constant, maximizing  $p(O | I)$  is equivalent to minimizing

$$J(O) = \frac{\| I - P * O \|^2}{2\sigma_n^2} \quad (13)$$

We obtain the least square solution using equation 5. This solution is not regularized. A regularization can be derived by minimizing equation 13 using an iterative algorithm such as the steepest descent minimization method. A typical iteration is

$$O^{n+1} = O^n + \gamma P^* * (I - P * O^n) \quad (14)$$

where  $P^*(x, y) = P(-x, -y)$ .  $P^*$  is the transpose of the PSF, and  $O^{(n)}$  is the current estimate of the desired “real image”. This method is usually called the Landweber method (Landweber 1951), but sometimes also the *successive approximations* or Jacobi method (Bertero and Boccacci 1998). The number of iterations plays an important role in these iterative methods. Indeed, the number of iterations can be considered as a regularization parameter. When the number of iterations increases, the iterates first approach the unknown object, and then potentially go away from it (Bertero and Boccacci 1998). Furthermore some constraints can be incorporated easily in the basic iterative scheme. Commonly used constraints are the positivity (i.e. the object must be positive), the support constraint (i.e. the object belongs to a given spatial domain), or the band-limited constraint (i.e the Fourier transform of the object belongs to a given frequency domain). More generally the constrained Landweber method is written as:

$$O^{n+1} = \mathcal{P}_C[O^n + \alpha(I - P * O^n)] \quad (15)$$

where  $\mathcal{P}_C$  is the projection operator which enforces our set of constraints on  $O^n$ .

### 5.3. Gaussian Bayes Model

If the object and the noise are assumed to follow Gaussian distributions with zero mean and variance respectively equal to  $\sigma_O$  and  $\sigma_N$ , then a Bayes solution leads to the Wiener filter:

$$\hat{O}(u, v) = \frac{\hat{P}^*(u, v)\hat{I}(u, v)}{|\hat{P}(u, v)|^2 + \frac{\sigma_N^2(u, v)}{\sigma_O^2(u, v)}} \quad (16)$$

Wiener filtering has serious drawbacks (artifact creation such as ringing effects), and needs spectral noise estimation. Its advantage is that it is very fast.

### 5.4. Maximum Likelihood with Poisson Noise

The probability  $p(I | O)$  is

$$p(I | O) = \prod_{x, y} \frac{((P * O)(x, y))^{I(x, y)} \exp\{-(P * O)(x, y)\}}{I(x, y)!} \quad (17)$$

The maximum can be computed by taking the derivative of the logarithm:

$$\frac{\partial \ln p(I | O)(x, y)}{\partial O(x, y)} = 0 \quad (18)$$

Assuming the PSF is normalized to unity, and using Picard iteration (Issacson and Keller 1966), we get

$$O^{n+1}(x, y) = \left[ \frac{I(x, y)}{(P * O^n)(x, y)} * P^*(x, y) \right] O^n(x, y) \quad (19)$$

which is the Richardson-Lucy algorithm (Richardson 1972; Lucy 1974; Shepp and Vardi 1982), also sometimes called the *expectation maximization* or EM method (Dempster et al. 1977). This method is commonly used in astronomy. Flux is preserved and the solution is always positive. Constraints can also be added by using the following iterative scheme:

$$O^{n+1} = \mathcal{P}_C \left[ O^n \left[ \frac{I}{(P * O^n)} * P^* \right] \right] \quad (20)$$

### 5.5. Poisson Bayes Model

We formulate the object PDF (probability density function) as

$$p(O) = \prod_{x,y} \frac{M(x, y)^{O(x,y)} \exp\{-M(x, y)\}}{O(x, y)!} \quad (21)$$

The MAP solution is

$$O(x, y) = M(x, y) \exp \left\{ \left[ \frac{I(x, y)}{(P * O)(x, y)} - 1 \right] * P^*(x, y) \right\} \quad (22)$$

and choosing  $M = O^n$  and using Picard iteration leads to

$$O^{n+1}(x, y) = O^n(x, y) \exp \left\{ \left[ \frac{I(x, y)}{(P * O^n)(x, y)} - 1 \right] * P^*(x, y) \right\} \quad (23)$$

### 5.6. Maximum Entropy Method

In the absence of any information on the solution  $O$  except its positivity, a possible course of action is to derive the probability of  $O$  from its entropy, which is defined from information theory. Then if we know the entropy  $H$  of the solution, we derive its probability as

$$p(O) = \exp(-\alpha H(O)) \quad (24)$$

The most commonly used entropy functions are:

- Burg (1978):  $H_b(O) = -\sum_x \sum_y \ln(O(x, y))$
- Frieden (1978):  $H_f(O) = -\sum_x \sum_y O(x, y) \ln(O(x, y))$
- Gull and Skilling (1991):

$$H_g(O) = \sum_x \sum_y O(x, y) - M(x, y) - O(x, y) \ln(O(x, y)|M(x, y))$$

The last definition of the entropy has the advantage of having a zero maximum when  $O$  equals the model  $M$ , usually taken as a flat image.

### 5.7. Other Regularization Models

In this section, we discuss approaches to deconvolving images of extended objects.

Molina et al. (2001) present an excellent review of taking the spatial context of image restoration into account. Some appropriate prior is used for this. One such regularization constraint is:

$$\|CI\|^2 = \sum_x \sum_y I(x, y) - \frac{1}{4}(I(x, y+1) + I(x, y-1) + I(x+1, y) + I(x-1, y)) \quad (25)$$

Similar to the discussion above in section 5.2, this is equivalent to defining the prior

$$p(O) \propto \exp \left\{ -\frac{\alpha}{2} \|CI\|^2 \right\} \quad (26)$$

Given the form of equation 25, such regularization can be viewed as setting a constraint on the Laplacian of the restoration. In statistics this model is a simultaneous autoregressive model, SAR (Ripley 1981).

Alternative prior models can be defined, related to the SAR model of equation 25. In

$$p(O) \propto \exp \left\{ -\alpha \sum_x \sum_y (I(x, y) - I(x, y+1))^2 + (I(x, y) - I(x+1, y))^2 \right\} \quad (27)$$

constraints are set on first derivatives.

Blanc-Féraud and Barlaud (1996), and Charbonnier et al. (1997) consider the following prior:

$$p(O) \propto \exp \left\{ -\alpha \sum_x \sum_y \phi(\|\nabla I\|(x, y)) \right\} \quad (28)$$

$$\propto \exp \left\{ -\alpha \sum_x \sum_y (\phi(I(x, y) - I(x, y + 1))^2 + \phi(I(x, y) - I(x + 1, y))^2)^{\frac{1}{2}} \right\} \quad (29)$$

The function  $\phi$ , called *potential function*, is an edge preserving function. The term  $\alpha \sum_x \sum_y \phi(\|\nabla I\|(x, y))$  can also be interpreted as the Gibbs energy of a Markov Random Field.

The ARTUR method (Charbonnier et al. 1997), which has been used for helioseismic inversion (Corbard et al. 1999), uses the function  $\phi(t) = \log(1 + t^2)$ . Anisotropic diffusion (Perona and Malik 1990; Alvarez et al. 1992) uses similar functions, but in this case the solution is computed using *partial differential equations*.

The function  $\phi(t) = t$  leads to the *total variation* method (Rudin et al. 1992; Acar and Vogel 1994), the constraints are on first derivatives, and the model is a special case of a conditional autoregressive or CAR model. Molina et al. (2001) discuss the applicability of CAR models to image restoration involving galaxies. They argue that such models are particularly appropriate for the modeling of luminosity exponential and  $r^{1/4}$  laws.

The priors reviewed above can be extended to more complex models. In Molina et al. (1996) and Molina. et al. (2000), a compound Gauss Markov random field (CGMRF) model is used, one of the main properties of which is to target the preservation and improvement of line processes.

Another prior again was used in Molina and Cortijo (1992) for the case of planetary images.

## 6. Wavelet-Based Deconvolution

### 6.1. Introduction

The regularized methods presented in the previous sections give rise to a range of limitations: Fourier-based methods such as Wiener or Tikhonov methods lead to a band-limited solution, which is generally not optimal for astronomical image restoration, especially when the data contain point sources. The CLEAN method cannot correctly restore extended sources. The MEM method cannot recover simultaneously both compact and extended sources. MEM regularization presents several drawbacks, which are discussed in (Starck

et al. 2001b). The main problems are: (i) results depend on the background level, (ii) the proposed entropy functions give poor results for negative structures, i.e. structures under the background level (such as absorption bands in a spectrum), (iii) spatial correlation in the images is not taken into account. Iterative regularized methods such as Richardson-Lucy or the Landweber method do not prevent noise amplification during the iterations. Finally, if Markov Random Field based methods can be very useful for images with edges such as planetary images, they are ill-adapted for other cases, insofar as the majority of astronomical images contain objects which are relatively diffuse and do not have a “border”.

## 6.2. Towards Multiresolution

The Fourier domain diagonalizes the convolution operator, and we can identify and reduce the noise which is amplified during the inversion. When the signal can be modeled as stationary and Gaussian, the Wiener filter is optimal. But when the signal presents spatially localized features such as singularities or edges, these features cannot be well-represented with Fourier basis functions, which extend over the entire spatial domain. Other basis functions, such as wavelets, are better-suited to represent a large class of signals.

The wavelet transform, its conceptual links with Fourier and Gabor transforms, its indirect links with Karhunen-Loève and other transforms, and its generalization to multiresolution transforms, are all dealt with at length in (Starck et al. 1998a; Starck and Murtagh 2002) and many articles in the mainstream astronomy literature. Perhaps among the most important properties of the wavelet transform are the following:

- A resolution scale decomposition of the data is provided, using high-pass, band-pass or detail, and low-pass or smooth coefficients.
- The transformed data is more compact than the original. Indeed the noise is uniformly distributed over all coefficients while the signal of interest is concentrated in a few coefficients. Therefore, the signal-to-noise ratio of these coefficients is high, which opens the way towards data filtering and denoising.
- Of even greater relevance for data denoising, noise models defined for the original data often carry over well into wavelet transform space.

The last point is of tremendous importance in the physical sciences: due to the instrument or sensor used, we generally know the noise model we are dealing with. Direct definition

of this noise model’s parameters from the observed data is not at all easy. Determining the noise parameters in wavelet space is a far more effective procedure.

In this short briefing on the capital reasons explaining the importance of wavelet and multiresolution transforms, we note that wavelet transforms differ in the wavelet function used, and in a few different schemes for arranging the high and low frequency information used to define our data in wavelet space. Such schemes include the graphical “frequency domain tiling” used below in sections 6.3 and 6.4, which provide powerful summaries of transform properties. We have generally espoused so-called redundant transforms (i.e., each wavelet resolution scale has exactly the same number of pixels as the original data) whenever “pattern recognition” uses of the wavelet scale are uppermost in our minds, as opposed to compression.

A final point to note: the manner in which the wavelet transform is incorporated into more traditional deconvolution approaches varies quite a bit. In CLEAN, the scale-based decomposition is used to help us focus in on the solution. In section 6.4 below, the question of how noise is propagated into multiresolution transform space is uppermost in our minds. In section 6.5, we “siphon off” part of the restored data at each iteration of an iterative deconvolution, clean it by denoising, and feed it back into the following iteration.

We will return below to look at particular wavelet transform algorithms. In the remainder of this section we will review various approaches which have links or analogies with multiresolution approaches.

The concept of multiresolution was first introduced for deconvolution by Wakker and Schwarz (1988) when they proposed the Multiresolution CLEAN algorithm for interferometric image deconvolution. During the last ten years, many developments have taken place in order to improve the existing methods (CLEAN, Landweber, Lucy, MEM, and so on), and these results have led to the use of different levels of resolution.

The Lucy algorithm was modified (Lucy 1994) in order to take into account a priori information about stars in the field where both position and brightness are known. This is done by using a two-channel restoration algorithm, one channel representing the contribution relative to the stars, and the second to the background. A smoothness constraint is added on the background channel. This method, called *PLUCY*, was then refined firstly (and called *CPLUCY*) for considering subpixel positions (Hook 1999), and a second time (Pirzkal et al. 2000) (and called *GIRA*) for modifying the smoothness constraint.

A similar approach has been followed by Magain et al. (1998), but more in the spirit of the CLEAN algorithm. Again, the data are modeled as a set of point sources on top of spatially varying background, leading to a two-channel algorithm.

The MEM method has also been modified by several authors (Weir 1992; Bontekoe et al. 1994; Pantin and Starck 1996; Núñez and Llacer 1998; Starck et al. 2001b). First, Weir proposed the *Multi-channel MEM* method, in which an object is modeled as the sum of objects at different levels of resolution. The method was then improved by Bontekoe et al. (1994) with the *Pyramid MEM*. In particular, many regularization parameters were fixed by the introduction of the dyadic pyramid. The link between *Pyramid MEM* and wavelets was underlined in (Pantin and Starck 1996; Starck et al. 2001b), and it was shown that all the regularization parameters can be derived from the noise modeling. Wavelets were also used in (Núñez and Llacer 1998) in order to create a segmentation of the image, each region being then restored with a different smoothness constraint, depending on the resolution level where the region was found. This last method has however the drawback of requiring user interaction for deriving the segmentation threshold in the wavelet space.

The *Pixon* method (Dixon et al. 1996; Puetter and Yahil 1999) is relatively different to the previously described methods. This time, an object is modeled as the sum of pseudo-images smoothed locally by a function with position-dependent scale, called the *pixon* shape function. The set of pseudo-images defines a dictionary, and the image is supposed to contain only features included in this dictionary. But the main problem lies in the fact that features which cannot be detected directly in the data, nor in the data after a few Lucy iterations, will not be modeled with the *pixon* functions, and will be strongly regularized as background. The result is that the faintest objects are over-regularized while strong objects are well restored. This is striking in the example shown in Fig. 8.

Wavelets offer a mathematical framework for the multiresolution processing. Furthermore, they furnish an ideal way to include noise modeling in the deconvolution methods. Since the noise is the main problem in deconvolution, wavelets are very well adapted to the regularization task.

### 6.3. The Wavelet Transform

We begin with the wavelet transform used in the overwhelming majority of practical applications, for the simple reason that its performance in compression is well-proven. It is used in the JPEG2000 standard, for instance. Of course, for compression, it is a non-redundant transform. The schema used in the wavelet transform output, and the associated frequency domain tiling, will be familiar to anyone who has studied wavelets in the non-astronomy (and compression) context. In section 6.4, we will contrast the bi-orthogonal wavelet transform with the recently developed, innovative use of the wavelet-vaguelette approach to noise filtering.



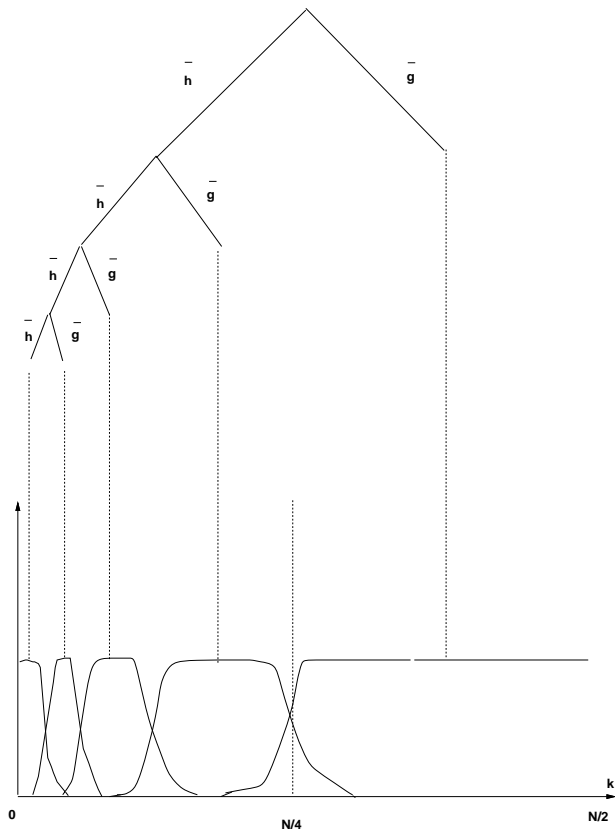


Fig. 2.— Frequency domain tiling by the 1D wavelet transform. The filter pair,  $\bar{h}$  and  $\bar{g}$ , are respectively low-pass and band-pass. The tree shows the order of application of these filters. The tiling shows where these filters have an effect in frequency space.

We denote  $\mathcal{W}$  the (bi-) orthogonal wavelet transform, and  $w$  the wavelet transform of a signal  $s$ :  $w = \mathcal{W}s$ .  $w$  is composed of a set of wavelet bands  $w_j$  and a coarse version  $c_J$  of  $s$ ,  $w = \{w_1, \dots, w_J, c_J\}$ , where  $J$  is the number of scales used in the wavelet transform. Roughly speaking, the Fourier transform of a given wavelet band  $w_j$  is localized in a frequency band with support  $[\frac{1}{2^{j+1}}, \frac{1}{2^j}]$ , and the Fourier transform of the smoothed array  $c_J$  is localized in the frequency band with support  $[0, \frac{1}{2^J}]$ . Thus, the algorithm outputs  $J + 1$  subband arrays. The indexing is such that, here,  $j = 1$  corresponds to the finest scale (high frequencies). Coefficients  $c_{j,l}$  and  $w_{j,l}$  are obtained by means of the filters  $h$  and  $g$ ,  $c_{j+1,l} = \sum_k h(k - 2l)c_{j,k}$  and  $w_{j+1,l} = \sum_k g(k - 2l)c_{j,k}$ . where the filters  $h$  and  $g$  are derived from the analysis wavelet function  $\psi$ .  $h$  and  $g$  can be interpreted as, respectively, a low and a high pass filter. Another important point in this algorithm is the critical sampling. Indeed, the number of pixels in the transformed data  $w$  is equal to the number of pixels  $N$  in the original signal. This is possible because of the decimation performed at each resolution level. The signal  $c_j$  at

resolution level  $j$  (with  $N_j$  pixels and  $c_0 = s$ ) is decomposed into two bands  $w_{j+1}$  and  $c_{j+1}$ , both of them containing  $\frac{N_j}{2}$  pixels. Finally, the signal  $s$  can be reconstructed from its wavelet coefficients:  $s = \mathcal{W}^{-1}w$  using the inverse wavelet transform.

Fig. 2 shows the frequency domain tiling by the 1D wavelet transform. The first convolution step by the two filters  $h$  and  $g$  separates the frequency band into two parts, the high frequencies and the low frequencies. The first scale  $w_1$  of the wavelet transform corresponds to the high frequencies. The same process is then repeated several times on the low frequency band, which is separated into two parts at each step. We get the wavelet scales  $w_2, \dots, w_J$  and  $c_J$ . The wavelet transform can be seen as a set of pass-band filters which has the properties of being reversible (the original data can be reconstructed from the wavelet coefficients) and non-redundant.

The two-dimensional algorithm is based on separate variables leading to prioritizing of horizontal, vertical and diagonal directions. The detail signal is obtained from three wavelets: the vertical wavelet, the horizontal wavelet, and the diagonal wavelet. This leads to three wavelet subimages at each resolution level. This transform is non-redundant, which means that the number of pixels in the wavelet transformed data is the same as in the input data.

$f^{(2)}$	H. D. $j=2$	Horiz. Det. $j=1$	Horizontal Details $j=0$
V. D. $j=2$	D. D. $j=2$		
Vert. Det. $j=1$		Diag. Det. $j=1$	Diagonal Details $j=0$
Vertical Details $j=0$			

Fig. 3.— Orthogonal wavelet transform representation of an image.

Fig. 3 shows the spatial representation of a 2D wavelet transform. The first step decomposes the image into three wavelet coefficient bands (i.e horizontal band, vertical band and diagonal band), and the smoothed array. The same process is then repeated on the smoothed array.

Figure 4 shows the wavelet transform of a galaxy (NGC 2997) using four resolution

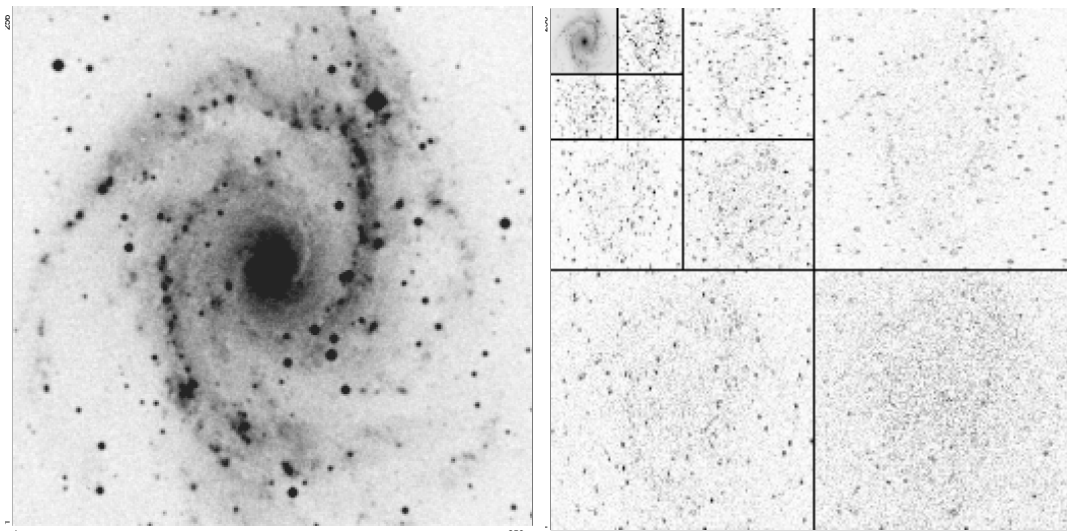


Fig. 4.— Galaxy NGC 2997 and its bi-orthogonal wavelet transform.

levels.

Other discrete wavelet transforms exist. The à trous wavelet transform is very well-suited for astronomical data and has been discussed in many papers and books (Starck et al. 1998a). By using the à trous wavelet transform algorithm, an image  $I$  can be defined as the sum of its  $J$  wavelet scales and the last smooth array:  $I(x, y) = c_J(x, y) + \sum_{j=1}^J w_{j,x,y}$  where the first term on the right is the last smoothed array, and  $w$  denotes a wavelet scale. This algorithm is quite different from the previous one. It is redundant, i.e. the number of pixels in the transformed data is larger than in the input data (each wavelet scale has the same size as the original image, hence the redundancy factor is  $J + 1$ ), and it is isotropic (there are no favored orientations). Both properties are useful for the purpose of astronomical image restoration.

Fig. 5 shows the à trous transform of the galaxy NGC 2997. Three wavelet scales are shown (upper left, upper right, lower left) and the final smoothed plane (lower right). The original image is given exactly by the sum of these four images.

Since the wavelet transform is a linear transform, the noise behavior in wavelet space can be well understood and correctly modeled. This point is fundamental since one of the main problems of deconvolution is the presence of noise in the data.

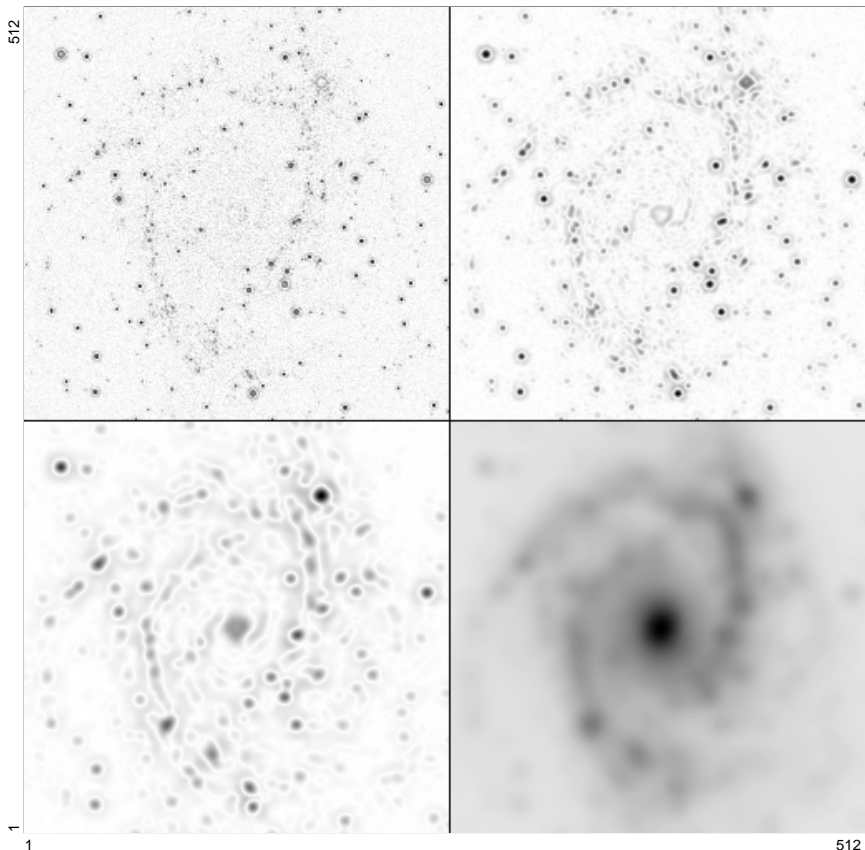


Fig. 5.— Wavelet transform of NGC 2997 by the à trous algorithm.

#### 6.4. Wavelet-Vaguelette Decomposition

The Wavelet-Vaguelette decomposition, proposed by Donoho (1995), consists of first applying an inverse filtering:

$$F = P^{-1} * I + P^{-1} * N = O + Z \quad (30)$$

where  $P^{-1}$  is the inverse filter ( $\hat{P}^{-1}(u, v) = \frac{1}{\hat{P}(u, v)}$ ). The noise  $Z = P^{-1} * N$  is not white but remains Gaussian. It is amplified when the deconvolution problem is unstable. Then, a wavelet transform is applied to  $F$ , the wavelet coefficients are soft- or hard-thresholded (Donoho 1993), and the inverse wavelet transform furnishes the solution.

The method has been refined by adapting the wavelet basis to the frequency response of the inverse of  $P$  (Kalifa 1999; Kalifa et al. 2000). This *Mirror Wavelet Basis* has a time-frequency tiling structure different from conventional wavelets, and isolates the frequency

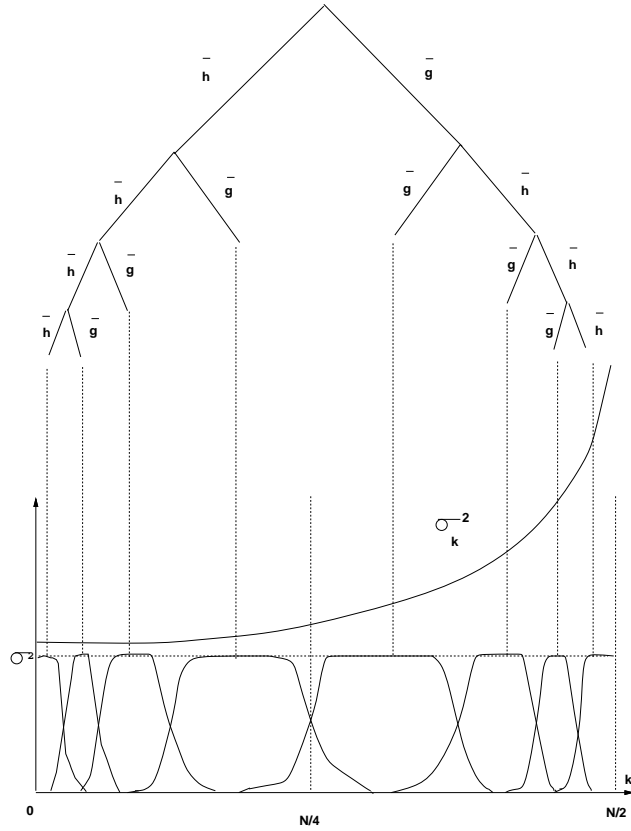


Fig. 6.— Frequency domain tiling using a wavelet packet decomposition with a mirror basis. The variance of the noise has a hyperbolic growth. See text for discussion of the implications of the noise variation.

where  $\hat{P}$  is close to zero, because a singularity in  $\hat{P}^{-1}(u_s, v_s)$  influences the noise variance in the wavelet scale corresponding to the frequency band which includes  $(u_s, v_s)$ . Fig. 6 and Fig. 7 show the decomposition of the Fourier space respectively in 1D and 2D.

Because it may be not possible to isolate all singularities, Neelamani (1999) and Neelamani et al. (2001) advocated a hybrid approach, proposing to still use the Fourier domain so as to restrict excessive noise amplification. Regularization in the Fourier domain is carried out with the window function  $W_\lambda$ :

$$\hat{W}_\lambda(u, v) = \frac{|\hat{P}(u, v)|^2}{|\hat{P}(u, v)|^2 + \lambda \mathcal{T}(u, v)} \quad (31)$$

where  $\mathcal{T}(u, v) = \frac{\sigma^2}{\hat{S}(u, v)}$ ,  $S$  being the power spectral density of the observed signal.

$$F = W_\lambda * P^{-1} * I + W_\lambda * P^{-1} * N \quad (32)$$

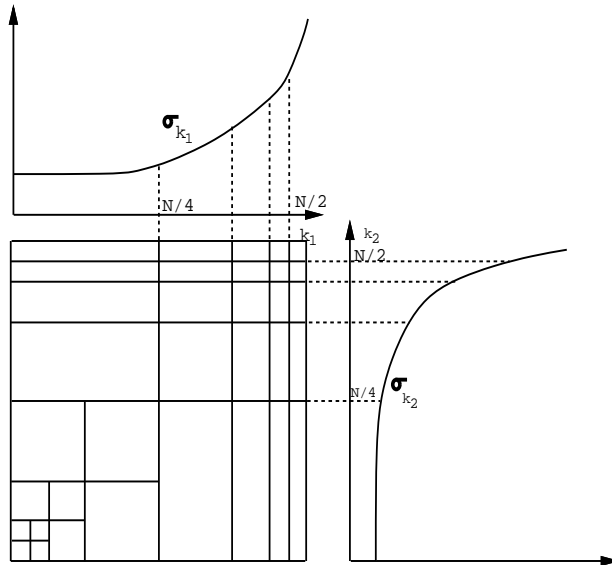


Fig. 7.— The mirror wavelet basis in 2-dimensional space. See text for discussion of the implications of the noise variation.

The regularization parameter  $\lambda$  controls the amount of Fourier-domain shrinkage, and should be relatively small ( $< 1$ ) (Neelamani et al. 2001). The estimate  $F$  still contains some noise, and a wavelet transform is performed to remove the remaining noise. The optimal  $\lambda$  is determined using a given cost function. See (Neelamani et al. 2001) for more details.

This approach is fast and competitive compared to linear methods, and the wavelet thresholding removes the Gibbs oscillations. It presents however several drawbacks:

1. The regularization parameter is not so easy to find in practice (Neelamani et al. 2001), and requires some computation time, which limits the usefulness of the method.
2. The positivity a priori is not used.
3. The power spectrum of the observed signal is generally not known.
4. It is not trivial to consider non-Gaussian noise.

The second point is important for astronomical images. It is well-known that the positivity constraint has a strong influence on the solution quality (Kempen and van Vliet 2000). We will see in the following that it is straightforward to modify the standard iterative methods in such a way that they benefit from the capacity of wavelets to separate the signal from the noise.

## 6.5. Regularization from the Multiresolution Support

### 6.5.1. Noise suppression based on the wavelet transform

We have noted how, in using an iterative deconvolution algorithm such as Van Cittert or Richardson-Lucy, we define  $R^{(n)}(x, y)$ , the residual at iteration  $n$ :

$$R^n(x, y) = I(x, y) - (P * O^n)(x, y) \quad (33)$$

By using the à trous wavelet transform algorithm,  $R^n$  can be defined as the sum of its  $J$  wavelet scales and the last smooth array:

$$R^n(x, y) = c_J(x, y) + \sum_{j=1}^J w_{j,x,y} \quad (34)$$

where the first term on the right is the last smoothed array, and  $w$  denotes a wavelet scale.

The wavelet coefficients provide a mechanism to extract only the significant structures from the residuals at each iteration. Normally, a large part of these residuals are statistically non-significant. The significant residual (Murtagh and Starck 1994; Starck and Murtagh 1994) is then:

$$\bar{R}^n(x, y) = c_{J,x,y} + \sum_{j=1}^J M(j, x, y)w_{j,x,y} \quad (35)$$

where  $M(j, x, y)$  is the multiresolution support, and is defined by:

$$M(j, x, y) = \begin{cases} 1 & \text{if } w_{j,x,y} \text{ is significant} \\ 0 & \text{if } w_{j,x,y} \text{ is non-significant} \end{cases} \quad (36)$$

This describes in a logical or Boolean way if the data contains information at a given scale  $j$  and at a given position  $(x, y)$ . Assuming that the noise follows a given distribution,  $w_j(x, y)$  is significant if the probability that the wavelet coefficient is due to noise is small ( $P(|W > w_{j,x,y}|) < \epsilon$ ). In the case of Gaussian noise,  $w_{j,x,y}$  is significant if  $w_{j,x,y} > k\sigma_j$ , where  $\sigma_j$  is the noise standard deviation at scale  $j$ , and  $k$  is a constant, generally taken between 3 and 5. Different noise models are discussed in (Starck et al. 1998a). If a priori information is available, such as star positions, it can easily be introduced into the multiresolution support.

An alternative approach was outlined in (Murtagh et al. 1995) and (Starck et al. 1995): the support was initialized to zero, and built up at each iteration of the restoration algorithm.

Thus in equation (35) above,  $M(j, x, y)$  was additionally indexed by  $n$ , the iteration number. In this case, the support was specified in terms of significant pixels at each scale,  $j$ ; and in addition pixels could become significant as the iterations proceeded, but could not be made non-significant.

### 6.5.2. Regularization of Van Cittert's algorithm

Van Cittert's iteration (Cittert 1931) is:

$$O^{n+1}(x, y) = O^n(x, y) + \alpha R^n(x, y) \quad (37)$$

with  $R^n(x, y) = I^n(x, y) - (P * O^n)(x, y)$ . Regularization using significant structures leads to:

$$O^{n+1}(x, y) = O^n(x, y) + \alpha \bar{R}^n(x, y) \quad (38)$$

The basic idea of this regularization method consists of detecting, at each scale, structures of a given size in the residual  $R^n(x, y)$  and putting them in the restored image  $O^n(x, y)$ . The process finishes when no more structures are detected. Then, we have separated the image  $I(x, y)$  into two images  $\tilde{O}(x, y)$  and  $R(x, y)$ .  $\tilde{O}$  is the restored image, which ought not to contain any noise, and  $R(x, y)$  is the final residual which ought not to contain any structure.  $R$  is our estimate of the noise  $N(x, y)$ .

### 6.5.3. Regularization of the one-step gradient method

The one-step gradient iteration is:

$$O^{n+1}(x, y) = O^n(x, y) + P^*(x, y) * R^n(x, y) \quad (39)$$

with  $R^n(x, y) = I(x, y) - (P * O^n)(x, y)$ . Regularization by significant structures leads to:

$$O^{n+1}(x, y) = O^n(x, y) + P^*(x, y) * \bar{R}^n(x, y) \quad (40)$$

### 6.5.4. Regularization of the Richardson-Lucy algorithm

From equation (1), we have  $I^n(x, y) = (P * O^n)(x, y)$ . Then  $R^n(x, y) = I(x, y) - I^n(x, y)$ , and hence  $I(x, y) = I^n(x, y) + R^n(x, y)$ .



The Richardson-Lucy equation is:

$$O^{n+1}(x, y) = O^n(x, y) \left[ \frac{I^n(x, y) + R^n(x, y)}{I^n(x, y)} * P^*(x, y) \right]$$

and regularization leads to:

$$O^{n+1}(x, y) = O^n(x, y) \left[ \frac{I^n(x, y) + \bar{R}^n(x, y)}{I^n(x, y)} * P^*(x, y) \right]$$

### 6.5.5. Convergence

The standard deviation of the residual decreases until no more significant structures are found. Convergence can be estimated from the residual. The algorithm stops when a user-specified threshold is reached:

$$(\sigma_{R^{n-1}} - \sigma_{R^n}) / (\sigma_{R^n}) < \epsilon \tag{41}$$

### 6.5.6. Examples

A simulated Hubble Space Telescope Wide Field Camera image of a distant cluster of galaxies is shown in Fig. 8, upper left. The image used was one of a number described in (Caulet and Freudling 1993; Freudling and Caulet 1993). The simulated data are shown in Fig. 8, upper right. Four deconvolution methods were tested: Richardson-Lucy, Pixon, wavelet-vaguelette, Wavelet-Lucy. Deconvolved images are presented respectively in Fig. 8 middle left, middle right, bottom left and right. The Richardson-Lucy method amplifies the noise, which implies that the faintest objects disappear in the deconvolved image. The Pixon method introduces regularization, and the noise is under control, while objects where “pixon” have been detected are relatively well-protected from the regularization effect. Since the “pixon” features are detected from noisy partially deconvolved data, the faintest objects are not in the pixon map and are strongly regularized. The wavelet-vaguelette method is very fast and produces relatively high quality results when compared to Pixon or Richardson-Lucy, but the Wavelet-Lucy method seems clearly the best of the four methods. There are fewer spurious objects than in the wavelet-vaguelette method, it is stable for any kind of PSF, and any kind of noise modeling can be considered.

## 6.6. Wavelet CLEAN

The CLEAN solution is only available if the image does not contain large-scale structures. Wakker and Schwarz (1988) introduced the concept of Multiresolution Clean (MRC) in order to alleviate the difficulties occurring in CLEAN for extended sources. The MRC approach consists of building two intermediate images, the first one (called the smooth map) by smoothing the data to a lower resolution with a Gaussian function, and the second one (called the difference map) by subtracting the smoothed image from the original data. Both these images are then processed separately. By using a standard CLEAN algorithm on them, the smoothed clean map and difference clean map are obtained. The recombination of these two maps gives the clean map at the full resolution. This algorithm may be viewed as an artificial recipe, but it has been shown (Starck et al. 1994; Starck and Bijaoui 1994; Starck et al. 1998a) that it is linked to multiresolution analysis. Wavelet analysis leads to a generalization of MRC from a set of scales. The Wavelet Clean Method (WCLEAN) consists of the following steps:

- Apply the wavelet transform to the image: we get  $W_I$ .
- Apply the wavelet transform to the PSF: we get  $W_P$ .
- Apply the wavelet transform to the Clean Beam: we get  $W_C$ .
- For each scale  $j$  of the wavelet transform, apply the CLEAN algorithm using the wavelet scale  $j$  of both  $W_I$  and  $W_P$ .
- Apply an iterative reconstruction algorithm using  $W_C$ .

More details can be found in (Starck et al. 1994, 1998a).

## 6.7. Multiscale Entropy

### 6.7.1. Introduction

In (Starck et al. 1998b; Starck and Murtagh 1999; Starck et al. 2001b), the benchmark properties for a good “physical” definition of entropy were discussed, and it was proposed to consider that the entropy of a signal is the sum of the information at each scale of its wavelet transform (Starck et al. 1998b), and the information of a wavelet coefficient is related to the probability of it being due to noise. Denoting  $h$  the information relative to a single wavelet coefficient, we have:  $H(X) = \sum_{j=1}^J \sum_{k=1}^{N_j} h(w_{j,k})$ , with  $h(w_{j,k}) = -\ln p(w_{j,k})$ .  $J$  is

the number of scales, and  $N_j$  is the number of samples (pixels, time- or wavelength-interval values) in band (scale)  $j$ . For Gaussian noise, the information is proportional to the energy of the wavelet coefficients. The larger the value of a normalized wavelet coefficient, then the lower will be its probability of being noise, and the higher will be the information furnished by this wavelet coefficient. Since  $H$  is corrupted by the noise, it can be decomposed into two components, one ( $H_s$ ) corresponding to the non-corrupted part, and the other ( $H_n$ ) to the corrupted part (Starck et al. 1998b):  $H(X) = H_s(X) + H_n(X)$ .  $H_s$  is called the signal information, and  $H_n$  the noise information. For each wavelet coefficient  $w_{j,k}$ , we have to estimate the proportions  $h_n$  and  $h_s$  of  $h$  (with  $h(w_{j,k}) = h_n(w_{j,k}) + h_s(w_{j,k})$ ) which should be assigned to  $H_n$  and  $H_s$ . Hence signal information and noise information are defined by

$$\begin{aligned} H_s(X) &= \sum_{j=1}^J \sum_{k=1}^{N_j} h_s(w_{j,k}) \\ H_n(X) &= \sum_{j=1}^J \sum_{k=1}^{N_j} h_n(w_{j,k}) \end{aligned} \quad (42)$$

If a wavelet coefficient is small, its value can be due to noise, and the information  $h$  relative to this single wavelet coefficient should be assigned to  $H_n$ . More details can be found in (Starck et al. 2001b).

Following the Bayesian scheme, the functional to minimize is:

$$J(O) = \sum_{k=1}^N \frac{(I_k - (P * O)_k)^2}{2\sigma_I^2} + \alpha \sum_{j=1}^J \sum_{k=1}^{N_j} \frac{w_{j,k}^2}{2\sigma_j^2} \quad (43)$$

where  $\sigma_j$  is the noise at scale  $j$ ,  $N_j$  the number of pixels at the scale  $j$ ,  $\sigma_I$  the noise standard deviation in the data, and  $J$  the number of scales.

Rather than minimizing the amount of information in the solution, we may prefer to minimize the amount of information which can be due to the noise. The function is now:

$$J(O) = \sum_{k=1}^N \frac{(I_k - (P * O)_k)^2}{2\sigma_I^2} + \alpha H_n(O) \quad (44)$$

and for Gaussian noise,  $H_n$  has been defined by

$$H_n(X) = \sum_{j=1}^J \sum_{k=1}^{N_j} \frac{1}{\sigma_j^2} \int_0^{|w_{j,k}|} u \operatorname{erf} \left( \frac{|w_{j,k}| - u}{\sqrt{2}\sigma_j} \right) \quad (45)$$

Minimizing  $H_n$  can be seen as a kind of adaptive soft-thresholding in the wavelet terminology. Finally, equation (44) can be generalized by (Starck et al. 2001b):

$$J(O) = H_s(I - P * O) + \alpha H_n(O) \quad (46)$$

i.e. we want to minimize the minimum of information due to the signal in the residual, and the minimum of information due to the noise in the solution.

### 6.7.2. Example: Beta Pictoris image deconvolution

The Beta Pictoris image (Pantin and Starck 1996) was obtained by integrating 5 hours on-source using a mid-infrared camera, TIMMI, placed on the 3.6 ESO telescope (La Silla, Chile). The raw image has a peak signal-to-noise ratio of 80. It is strongly blurred by a combination of seeing, diffraction (0.7 arcsec on a 3m class telescope) and additive Gaussian noise. The initial disk shape in the original image has been lost after the convolution with the PSF (see Fig. 9, top). Thus we need to deconvolve such an image to get the best information on this object i.e. the exact profile and thickness of the disk, and subsequently to compare the results to models of thermal dust emission.

After filtering (see Fig. 9, bottom left), the disk appears clearly. For detection of faint structures (the disk here), one can calculate that the application of such a filtering method to this image provides a gain of observing time of a factor of around 60. The deconvolved image (Fig. 9, bottom right) shows that the disk is extended at  $10 \mu\text{m}$  and asymmetrical. The multiscale entropy method is more effective for regularizing than other standard methods, and leads to good reconstruction of the faintest structures of the dust disk.

## 6.8. Summary of Scale-Based Deconvolution

As already mentioned, our objective in section 6 has been to take the major categories of deconvolution methods – linear inversion, CLEAN, Bayesian optimization, and maximum entropy (respectively sections 3, 4 and 5) – and seek where and how resolution scale information could be incorporated. A key requirement for us is that the basic method should stay the same in all cases (e.g. well-behaved convergence properties should remain well-behaved, new artifacts or other degradation must not be introduced, and so on). It follows that the essential properties of the methods described earlier (e.g., appropriateness of particular noise models, use or otherwise of particular a priori assumptions, etc.) hold in the multiple resolution setting also. We have cited examples of further reading on these enhanced methods.

## 7. Deconvolution and Resolution

In many cases, there is no sense in trying to deconvolve an image at the resolution of the pixel (especially when the PSF is very large). The idea to limit the resolution is relatively old, because it is already this concept which is used in the CLEAN algorithm (Högbom 1974). Indeed the clean beam fixes the resolution in the final solution. This principle was also developed by Lannes and Roques (1987) in a different form. This concept was re-invented, first by Gull and Skilling (1991) who called the clean beam the *Intrinsic Correlation Function* (ICF), and more recently by Magain et al. (1998) and Pijpers (1999).

The ICF is usually a Gaussian, but in some cases it may be useful to take another function. For example, if we want to compare two images  $I_1$  and  $I_2$  which are obtained with two wavelengths or with two different instruments, their PSFs  $P_1$  and  $P_2$  will certainly be different. The classic approach would be to deconvolve  $I_1$  with  $P_2$  and  $I_2$  with  $P_1$ , so we are sure that both are at the same resolution. But unfortunately we lose some resolution in doing this. Deconvolving both images is generally not possible because we can never be sure that both solutions  $O_1$  and  $O_2$  will have the same resolution.

A solution would be to deconvolve only the image which has the worse resolution (say  $I_1$ ), and to limit the deconvolution to the second image resolution ( $I_2$ ). Then, we just have to take  $P_2$  for the ICF. The deconvolution problem is to find  $\tilde{O}$  (hidden solution) such that:

$$I_1 = P_1 * P_2 * \tilde{O} \tag{47}$$

and our real solution  $O_1$  at the same resolution as  $I_2$  is obtained by convolving  $\tilde{O}$  with  $P_2$ .  $O_1$  and  $I_2$  can then be compared.

Introducing an ICF  $G$  in the deconvolution equation leads to just considering a new PSF  $P'$  which is the convolution of  $P$  and  $G$ . The deconvolution is carried out using  $P'$ , and the solution must be reconvolved with  $G$  at the end. In this way, the solution has a constrained resolution, but aliasing may occur during the iterative process, and it is not sure that the artifacts will disappear after the re-convolution with  $G$ . Magain et al. (1998) proposed an innovative alternative to this problem, by assuming that the PSF can be considered as the convolution product of two terms, the ICF  $G$  and an unknown  $S$ ,  $P = G * S$ . Using  $S$  instead of  $P$  in the deconvolution process, and a sufficiently large FWHM value for  $G$ , implies that the Shannon sampling theorem (Shannon 1948) is never violated. But the problem is now to calculate  $S$ , knowing  $P$  and  $G$ , which is again a deconvolution problem. Unfortunately, this delicate point was not discussed in the original paper. Propagation of the error on the  $S$  estimation in the final solution has also until now not been investigated, even if this issue seems to be quite important.

## 8. Super-Resolution

### 8.1. Definition

Super-resolution consists of recovering object spatial frequency information outside the spatial bandwidth of the image formation system. In other terms, frequency components where  $\hat{P}(\nu) = 0$  have to be recovered. It has been demonstrated (Donoho et al. 1992) that this is possible under certain conditions. The observed object must be *nearly black*, i.e. nearly zero in all but a small fraction of samples. Denoting  $n$  the number of samples,  $m$  the number of non-zero values in the Fourier transform of the PSF, and  $\epsilon = \frac{m}{n}$  the incompleteness ratio, it has been shown that an image (Donoho et al. 1992):

- Must admit super-resolution if the object is  $\frac{1}{2}\epsilon$ -black.
- Might admit super-resolution if the object is  $\epsilon$ -black. In this case, it depends on the noise level and the spacing of non-zero elements in the object. Well-spaced elements favor the possibility of super-resolution.
- Cannot admit super-resolution if the object is not  $\epsilon$ -black.

Near blackness is both necessary and sufficient for super-resolution. Astronomical images often give rise to such data sets, where the real information (stars and galaxies) is contained in very few pixels. If the  $\frac{1}{2}\epsilon$ -blackness of the object is not verified, a solution is to limit the Fourier domain  $\Omega$  of the restored object. Several methods have been proposed in different contexts for achieving super-resolution.

### 8.2. Gerchberg-Saxon Papoulis Method

The Gerchberg-Saxon-Papoulis (Gerchberg 1974) method is iterative, and uses the a priori information on the object, which is its positivity and its support in the spatial domain. It was developed for interferometric image reconstruction, where we want to recover the object  $O$  from some of its *visibilities*, i.e. some of its frequency components. Hence, the object is supposed to be known in a given Fourier domain  $\Omega$  and we need to recover the object outside this domain. The problem can also be seen as a deconvolution problem,  $I = P * O$ , where

$$P(u, v) = \begin{cases} 1 & \text{if } (u, v) \in \Omega \\ 0 & \text{otherwise} \end{cases} \quad (48)$$

We denote  $\mathcal{P}_{C_s}$  and  $\mathcal{P}_{C_f}$  the projection operators in the spatial and the Fourier domain:

$$\begin{aligned}\mathcal{P}_{C_s}(X(x, y)) &= \begin{cases} X(x, y) & \text{if } (x, y) \in \mathcal{D} \\ 0 & \text{otherwise} \end{cases} \\ \mathcal{P}_{C_f}(\hat{X}(u, v)) &= \begin{cases} \hat{I}(u, v) = \hat{O}(u, v) & \text{if } (u, v) \in \Omega \\ 0 & \text{otherwise} \end{cases}\end{aligned}\quad (49)$$

The projection operator  $\mathcal{P}_{C_s}$  replaces by zero all pixel values which are not in the spatial support defined by  $\mathcal{D}$ , and  $\mathcal{P}_{C_f}$  replaces all frequencies in the Fourier domain  $\Omega$  by the frequencies of the object  $O$ . The Gerchberg algorithm is:

1. Compute  $\tilde{O}^0 =$  inverse Fourier transform of  $\hat{I}$ , and set  $i = 0$ .
2. Compute  $X_1 = \mathcal{P}_{C_s}(\tilde{O}^i)$ .
3. Compute  $\hat{X}_1 =$  Fourier transform of  $X_1$ .
4. Compute  $\hat{X}_2 = \mathcal{P}_{C_f}(\hat{X}_1)$ .
5. Compute  $X_2 =$  inverse Fourier transform of  $\hat{X}_2$ .
6. Compute  $\tilde{O}^{i+1} = \mathcal{P}_{C_s}(\hat{X}_2)$ .
7. Set  $X_1 = \tilde{O}^{i+1}$ ,  $i = i + 1$  and go to 2.

The algorithm consists just of forcing iteratively the solution to be zero outside the spatial domain  $\mathcal{D}$ , and equal to the observed visibilities inside the Fourier domain  $\Omega$ . It has been shown that this algorithm can be derived from the Landweber method (Bertero and Boccacci 1998), and therefore its convergence and regularization properties are the same as for the Landweber method. It is straightforward to introduce the positivity constraint by replacing  $\mathcal{P}_{C_s}$  by  $\mathcal{P}_{C_s}^+$

$$\mathcal{P}_{C_s}^+(X(x, y)) = \begin{cases} \max(X(x, y), 0) & \text{if } (x, y) \in \mathcal{D} \\ 0 & \text{otherwise} \end{cases}$$

The Gerchberg method can be generalized (Bertero and Boccacci 1998) using the Landweber iteration:

$$O^{n+1} = \mathcal{P}_{C_s}^+ [O^n + \alpha(P^* * L - P^* * P * O^n)] \quad (50)$$

where  $L = \mathcal{P}_{C_s}^+(I)$ .

### 8.3. Deconvolution with Interpolation

The MAP Poisson algorithm, combined with an interpolation, can be used to achieve super-resolution (Hunt 1994):

$$O^{n+1} = O^n \exp \left\{ \left( \frac{I}{(P * O^n)_\downarrow} - 1 \right)_\uparrow * P^* \right\} \quad (51)$$

where uparrow and downarrow notation describes respectively the oversampling and down-sampling operators. The PSF  $P$  must be sampled on the same grid as the object.

### 8.4. Undersampled Point Spread Function

When considering sampling, we should remember that detector pixels are “bins” for capturing flux, and hence that there is inherent area integration. At all times therefore signal detection implies signal convolution. Passing from one spatial resolution to another (which is implicit, for example, when cross-correlating signals from different detectors) necessarily involves deconvolution, however this is actually achieved in practice.

We now look at the case where observations are made with an undersampled PSF. When the observation is repeated several times with a small shift between two measurements, we can reconstruct a deconvolved image on a smaller grid. We denote  $D(i, j, k)$  the  $k$ th observation ( $k = 1 \dots n$ ),  $\Delta_{i,k}$ ,  $\Delta_{j,k}$  the shift in both directions relative to the first frame,  $\mathcal{L}_\uparrow$  the operator which coadds all the frame on a smaller grid, and  $\mathcal{L}_\downarrow^{-1}$  the operator which estimates  $D$  from  $\mathcal{L}_\uparrow D$  using shifting and averaging operations. The  $\Delta_{i,k}$ ,  $\Delta_{j,k}$  shifts are generally derived from the observations using correlation methods, or a PSF fitting (if a star is in the field), but can also be the jitter information if the data is obtained from space. Note also that  $\mathcal{L}_\downarrow^{-1} \mathcal{L}_\uparrow D \neq D$ . The point spread function  $P$  can generally be derived on a finer grid using a set of observations of a star, or using an optical modeling of the instrument. The deconvolution iteration becomes:

$$O^{n+1} = O^n + \alpha P^* [\mathcal{L}_\uparrow (D - \mathcal{L}_\downarrow^{-1} (P * O^n))] \quad (52)$$

and the positivity and spatial constraints can also be used:

$$O^{n+1} = \mathcal{P}_{C_s}^+ [O^n + \alpha P^* [\mathcal{L}_\uparrow (D - \mathcal{L}_\downarrow^{-1} (P * O^n))]] \quad (53)$$

The coaddition operator  $\mathcal{L}_\uparrow$  can be implemented in different ways. All frames can first be interpolated to the finer grid size, shifted using an interpolation function, and then coadded.



“Dithering” or “jitter” have been terms applied to purposeful use of offsets in imaging (Hook and Fruchter 2000). An ad-hoc method called “drizzling” is developed by Hook and Fruchter (2000) and implemented in IRAF, based on mapping pixels to a finer grid and assuming knowledge of geometric distortion.

Dithering may be described as a way of recovering Nyquist sampling. Moving the source image to get new samples is easy to understand, particularly with the effective PSF concept, where the effective PSF combines the native optical PSF and the areal integral within the detector. In recent work, (Gammaitoni et al. 1998) consider dithering as a special case of “stochastic resonance”, which in general seeks to amplify weak signals by the assistance of small quantities of noise.

Lauer (1999) ignores geometric distortion and instead addresses the problem of aliasing resulting from combining undersampled images. A linear combination of Fourier transforms of the offset images is used, which mitigates aliasing artifacts in direct space.

### 8.5. Multiscale Support Constraint

The constraint operator  $\mathcal{P}_{C_s}^+$  may not always be easy to determine, especially when the observed object is extended. Furthermore, if the object is very extended, the support will be very large and the support constraint may have very small influence on the final result. For this reason, it may be convenient to replace the support constraint by the multiresolution support constraint. The advantages are the following:

- It can be automatically calculated from the noise modeling in the wavelet space.
- Extended objects are generally also smooth. This means that the support on the small scales will be small, and therefore this introduces a smoothness constraint on extended objects, and no constraint on point-like objects.

## 9. Conclusions

We will conclude with a short look at how multiscale methods used in deconvolution are evolving and maturing.

We have seen that the recent improvement in deconvolution methods has led to use of multiscale approaches. These can be summarized as follows:

- Linear inverse filtering leading to wavelet-vaguelette decomposition.
- CLEAN leading to wavelet-CLEAN.
- |                     |   |                   |                                 |
|---------------------|---|-------------------|---------------------------------|
| Fixed step gradient | } | Regularization by |                                 |
| • Lucy              |   |                   | leading to: the multiresolution |
| Van Cittert         |   |                   |                                 |
- MEM leading to the multiscale entropy method.

The multiscale entropy method (Starck et al. 2001b), which generalized the wavelet regularized iterative methods, allows us to separate the deconvolution problem into two separate problems: noise control from one side, and solution smoothness control on the other side. The advantage of this approach is that noise control is better carried out in the image domain, while smoothness control can only be carried out in the object domain.

The reason for the success of wavelets is due to the fact that wavelet bases represent well a large class of signals. Other multiscale methods, such as the ridgelet or the curvelet transform (Candès and Donoho 1999, 2000; Donoho and Duncan 2000; Starck et al. 2001a) will certainly play a role in the future.

An old view of astronomy in practice is that of the observational specialist, aided by one or more data analysis specialists. This view is changing fast with the coming of astronomy “collaboratories”, supported by middleware and web services. Our review of deconvolution is addressed to the teams which are leading the evolution towards use of the Grid, and “virtual observatory”.

The “virtual observatory” in astronomy is premised on the fact that all usable astronomy data are digital. High performance information cross-correlation and fusion, and long-term availability of information, are required. The term “virtual” in this context means the use of reduced or processed online data.

A second and closely associated development is that of the Grid. The computational Grid is to provide an algorithmic and processing infrastructure for the virtual science of the future. The data Grid is to allow ready access to information from our tera and peta byte data stores. The information Grid is to provide active and dynamic retrieval of information, and not just pointers to where information might or might not exist.

The evolution of the way we do science, driven by these themes, is inextricably linked to the problem areas and often recently-developed algorithmic solutions surveyed in this article.

As just one address for further information on innovative developments is this broad area we give the following: iAstro, “Computational and Information Infrastructure in the Astronomical DataGrid”, <http://www.iAstro.org>. This is a 4-year (from late 2001) European collaborative project.

### *Acknowledgements*

We are grateful to an anonymous referee for various comments on an earlier version of this article.

## REFERENCES

- Acar, R. and Vogel, C.: 1994, *Physica D* **10**, 1217
- Adorf, H., Hook, R., and Lucy, L.: 1995, *International Journal of Imaging Systems and Technology* **6**, 339
- Alloin, D., Pantin, E., Lagage, P. O., and Granato, G. L.: 2000, *Astronomy and Astrophysics* **363**, 926
- Alvarez, L., Lions, P.-L., and Morel, J.-M.: 1992, *SIAM Journal on Numerical Analysis* **29**, 845
- Bertero, M. and Boccacci, P.: 1998, *Introduction to Inverse Problems in Imaging*, Institute of Physics
- Blanc-Féraud, L. and Barlaud, M.: 1996, *Vistas in Astronomy* **40**, 531
- Bontekoe, T., Koper, E., and Kester, D.: 1994, *Astronomy and Astrophysics* **284**, 1037
- Buonanno, R., Buscema, G., Corsi, C., Ferraro, I., and Iannicola, G.: 1983, *Astronomy and Astrophysics* **126**, 278
- Burg, J.: 1978, *Multichannel maximum entropy spectral analysis*, Annual Meeting International Society Exploratory Geophysics, Reprinted in *Modern Spectral Analysis*, D.G. Childers, ed., IEEE Press, 34–41

- Burud, I., Courbin, F., Magain, P., Lidman, C., Hutsemékers, D., Kneib, J.-P., Hjorth, J., Brewer, J., Pompei, E., Germany, L., Pritchard, J., Jaunsen, A. O., Letawe, G., and Meylan, G.: 2002, *A&A* **383**, 71
- Candès, E. and Donoho, D.: 1999, *Philosophical Transactions of the Royal Society of London A* **357**, 2495
- Candès, E. and Donoho, D.: 2000, in *SPIE conference on Signal and Image Processing: Wavelet Applications in Signal and Image Processing VIII*
- Caulet, A. and Freudling, W.: 1993, *ST-ECF Newsletter No. 20* pp 5–7
- Champagnat, F., Goussard, Y., and Idier, J.: 1996, *IEEE Transactions on Image Processing* **44**, 2988
- Charbonnier, P., Blanc-Féraud, L., Aubert, G., and Barlaud, M.: 1997, *IEEE Transactions on Image Processing* **6**, 298
- Christou, J. C., Bonnacini, D., Ageorges, N., and Marchis, F.: 1999, *The Messenger* **97**, 14
- Cittert, P. V.: 1931, *Zeitschrift für Physik* **69**, 298
- Corbard, T., Blanc-Féraud, L., Berthomieu, G., and Provost, J.: 1999, *Astronomy and Astrophysics* **344**, 696
- Cornwell, T.: 1989, in D. Alloin and J. Mariotti (eds.), *Diffraction-Limited Imaging with Very Large Telescopes*, Kluwer
- Courbin, F., Lidman, C., and Magain, P.: 1998, *Astronomy and Astrophysics* **330**, 57
- Coustenis, A., Gendron, E., Lai, O., Véran, J., Woillez, J., Combes, M., Vapillon, L., Fusco, T., Mugnier, L., and Rannou, P.: 2001, *Icarus* **154**, 501
- Dempster, A., Laird, N., and Rubin, D.: 1977, *Journal of the Royal Statistical Society, Series B* **39**, 1
- Dixon, D., Johnson, W., Kurfess, J., Pina, R., Puetter, R., Purcell, W., Tuemer, T., Wheaton, W., and Zych, A.: 1996, *Astronomy and Astrophysics, Supplement Series* **120**, 683
- Djorgovski, S.: 1983, *Journal of Astrophysics and Astronomy* **4**, 271
- Donoho, D.: 1993, *Proceedings of Symposia in Applied Mathematics* 47

- Donoho, D.: 1995, *Applied and Computational Harmonic Analysis* **2**, 101
- Donoho, D. and Duncan, M.: 2000, in H. Szu, M. Vetterli, W. Campbell, and J. Buss (eds.), *Proc. Aerosense 2000, Wavelet Applications VII*, Vol. 4056, pp 12–29, SPIE
- Donoho, D., Johnson, I., Hoch, J., and Stern, A.: 1992, *Journal of the Royal Statistical Society Series B* **47**
- Faure, C., Courbin, F., Kneib, J. P., Alloin, D., Bolzonella, M., and Burud, I.: 2002, *A&A* **386**, 69
- Freudling, W. and Caulet, A.: 1993, in P. Grosbøl (ed.), *Proceedings of the 5th ESO/ST-ECF Data Analysis Workshop*, pp 63–68, European Southern Observatory
- Frieden, B.: 1978, *Image Enhancement and Restoration*, Springer-Verlag
- Galatsanos, N. and Katsaggelos, A.: 1992, *IEEE Transactions on Image Processing* **1**, 322
- Gammaitoni, L., Hänggi, P., Jung, P., and Marchesoni, F.: 1998, *Reviews of Modern Physics* **70**, 223
- Gerchberg, R.: 1974, *Optica Acta* **21**, 709
- Golub, G., Heath, M., and Wahba, G.: 1979, *Technometrics* **21**, 215
- Gull, S. and Skilling, J.: 1991, *MEMSYS5 Quantified Maximum Entropy User's Manual*
- Hanisch, R. J. and White, R. L. (eds.): 1994, *The restoration of HST images and spectra - II*
- Högbom, J.: 1974, *Astronomy and Astrophysics Supplement Series* **15**, 417
- Hook, R.: 1999, *ST-ECF Newsletter No. 26* pp 3–5
- Hook, R. and Fruchter, A.: 2000, in *ASP Conference Series 216: Astronomical Data Analysis Software and Systems IX*, p. 521, Astronomical Society of the Pacific
- Hunt, B.: 1994, *International Journal of Modern Physics C* **5**, 151
- Issacson, E. and Keller, H.: 1966, *Analysis of Numerical Methods*, Wiley
- Kaarensen, K.: 1997, *IEEE Transactions on Image Processing* **45**, 1173
- Kalifa, J.: 1999, *Ph.D. thesis*, Ecole Polytechnique

- Kalifa, J., Mallat, S., and Rougé, B.: 2000, *Minimax Deconvolution in Mirror Wavelet Bases*, submitted
- Katsaggelos, A.: 1993, *Digital Image Processing*, Springer-Verlag
- Kempen, G. and van Vliet, L.: 2000, *Journal of the Optical Society of America A* **17**, 425
- Landweber, L.: 1951, *American Journal of Mathematics* **73**, 615
- Lannes, A. and Roques, S.: 1987, *Journal of the Optical Society of America* **4**, 189
- Lauer, T.: 1999, *Publications of the Astronomical Society of the Pacific* **111**, 227
- Lucy, L.: 1974, *Astronomical Journal* **79**, 745
- Lucy, L.: 1994, in R. J. Hanisch and R. L. White (eds.), *The Restoration of HST Images and Spectra II*, p. 79, Space Telescope Science Institute
- Magain, P., Courbin, F., and Sohy, S.: 1998, *Astrophysical Journal* **494**, 472
- Marchis, R., Prangé, R., and Christou, J.: 2000, *Icarus* **148**, 384
- Moffat, A.: 1969, *Astronomy and Astrophysics* **3**, 455
- Molina, R. and Cortijo, F.: 1992, in *Proc. International Conference on Pattern Recognition, ICPR'92*, Vol. 3, pp 147–150
- Molina, R., Katsaggelos, A., Mateos, J., and Abad, J.: 1996, *Vistas in Astronomy* **40**, 539
- Molina, R., Katsaggelos, A., Mateos, J., Hermoso, A., and Segall, A.: 2000, *Pattern Recognition* **33**, 555
- Molina, R., Núñez, J., Cortijo, F., and Mateos, J.: 2001, *IEEE Signal Processing Magazine* **18**, 11
- Molina, R., Ripley, B., Molina, A., Moreno, F., and Ortiz, J.: 1992, *Astrophysical Journal* **104**, 1662
- Murtagh, F. and Starck, J.: 1994, *ST-ECF Newsletter No. 21* pp 19–20
- Murtagh, F., Starck, J., and Bijaoui, A.: 1995, *Astronomy and Astrophysics, Supplement Series* **112**, 179
- Neelamani, R.: 1999, *Wavelet-based deconvolution for ill-conditioned systems*, MS thesis, Deptment of ECE, Rice University

- Neelamani, R., Choi, H., and Baraniuk, R. G.: 2001, *Wavelet-based deconvolution for ill-conditioned systems*, submitted
- Núñez, J. and Llacer, J.: 1998, *Astronomy and Astrophysics, Supplement Series* **131**, 167
- Pantin, E. and Starck, J.: 1996, *Astronomy and Astrophysics, Supplement Series* **315**, 575
- Perona, P. and Malik, J.: 1990, *IEEE Transactions on Pattern Analysis and Machine Intelligence* **12**, 629
- Pijpers, F. P.: 1999, *Monthly Notices of the Royal Astronomical Society* **307**, 659
- Pirzkal, N., Hook, R., and Lucy, L.: 2000, in N. Manset, C. Veillet, and D. Crabtree (eds.), *Astronomical Data Analysis Software and Systems IX*, p. 655, Astronomical Society of the Pacific
- Puetter, R. and Yahil, A.: 1999, in *ASP Conference Series 172: Astronomical Data Analysis Software and Systems VIII*, p. 307, Astronomical Society of the Pacific
- Radomski, J. T., Piña, R. K., Packham, C., Telesco, C. M., and Tadhunter, C. N.: 2002, *ApJ* **566**, 675
- Richardson, W.: 1972, *Journal of the Optical Society of America* **62**, 55
- Ripley, B.: 1981, *Spatial Statistics*, Wiley
- Rudin, L., Osher, S., and Fatemi, E.: 1992, *Physica D* **60**, 259
- Shannon, C.: 1948, *Bell System Technical Journal* **27**, 379
- Shepp, L. and Vardi, Y.: 1982, *IEEE Transactions on Medical Imaging* **MI-2**, 113
- Starck, J. and Bijaoui, A.: 1994, *Signal Processing* **35**, 195
- Starck, J., Bijaoui, A., Lopez, B., and Perrier, C.: 1994, *Astronomy and Astrophysics* **283**, 349
- Starck, J., Bijaoui, A., and Murtagh, F.: 1995, *CVGIP: Graphical Models and Image Processing* **57**, 420
- Starck, J., Candès, E., and Donoho, D.: 2001a, *IEEE Transactions on Image Processing*, to appear
- Starck, J. and Murtagh, F.: 1994, *Astronomy and Astrophysics* **288**, 343

- Starck, J. and Murtagh, F.: 1999, *Signal Processing* **76**, 147
- Starck, J. and Murtagh, F.: 2002, *Astronomical Image and Data Analysis*, Springer-Verlag, in press
- Starck, J., Murtagh, F., and Bijaoui, A.: 1998a, *Image Processing and Data Analysis: The Multiscale Approach*, Cambridge University Press
- Starck, J., Murtagh, F., and Gastaud, R.: 1998b, *IEEE Transactions on Circuits and Systems II* **45**, 1118
- Starck, J., Murtagh, F., Querre, P., and Bonnarel, F.: 2001b, *Astronomy and Astrophysics* **368**, 730
- Tikhonov, A., Goncharski, A., Stepanov, V., and Kochikov, I.: 1987, *Soviet Physics – Doklady* **32**, 456
- Wakker, B. and Schwarz, U.: 1988, *Annual Reviews of Astronomy and Astrophysics* **200**, 312
- Weir, N.: 1992, in D. Worrall, C. Biemesderfer, and J. Barnes (eds.), *Astronomical Data Analysis Software and System 1*, pp 186–190, Astronomical Society of the Pacific
- White, R. L. and Allen, R. J. (eds.): 1991, *The restoration of HST images and spectra*
- Zavagno, A., Lagage, P. O., and Cabrit, S.: 1999, *Astronomy and Astrophysics* **344**, 499



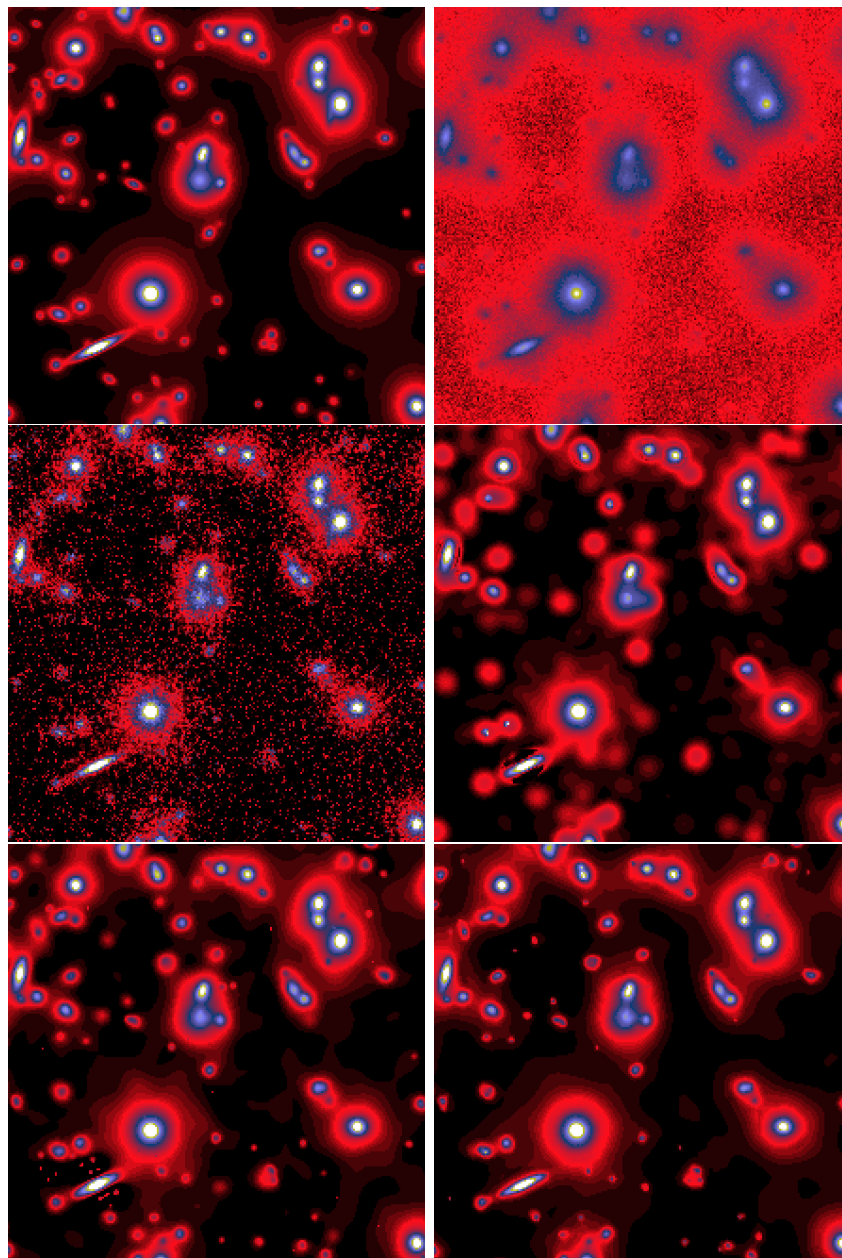


Fig. 8.— Simulated Hubble Space Telescope Wide Field Camera image of a distant cluster of galaxies. Six quadrants. Upper left: original, unaberrated and noise-free. Upper right: input, aberrated, noise added. Middle left: restoration, Richardson-Lucy. Middle right: restoration, Pixon method. Lower left, restoration wavelet-vaguelette. Lower right, restoration wavelet-Lucy.

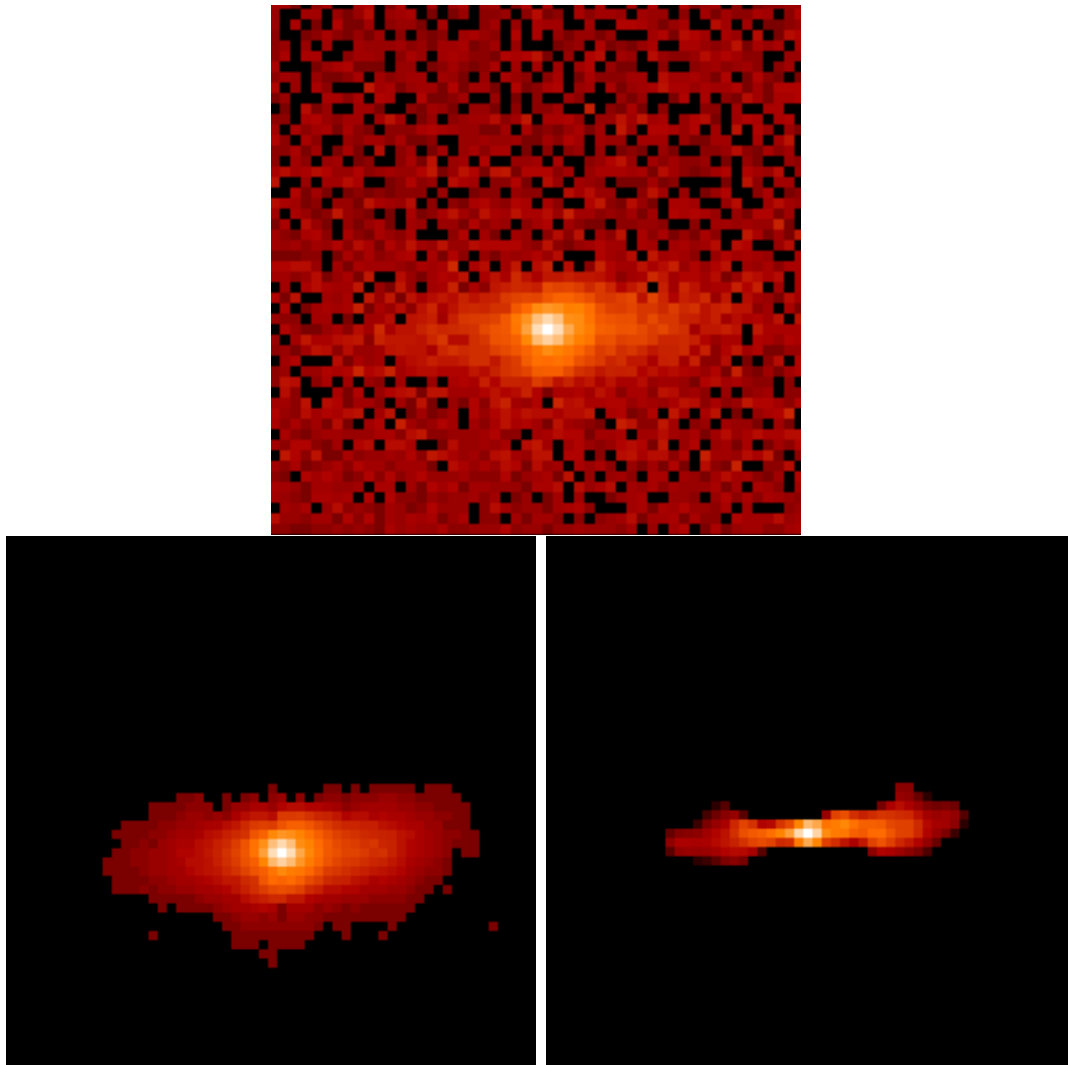


Fig. 9.— Top, Beta Pictoris raw data, bottom left, filtered image, and bottom right, deconvolved one.